Effective dose delivery in atmospheric pressure plasma jets for plasma medicine: a model predictive control approach

2017 Plasma Sources Sci. Technol. 26 085005

(http://iopscience.iop.org/0963-0252/26/8/085005)

IOP Publishing Plasma Sources Science and Technology
Plasma Sources Sci. Technol. **26** (2017) 085005 (15pp) https://doi.org/10.1088/1361-6595/aa7c5d

Effective dose delivery in atmospheric pressure plasma jets for plasma medicine: a model predictive control approach

Dogan Gidon, David B Graves and Ali Mesbah[1]

Department of Chemical and Biomolecular Engineering, University of California, Berkeley, CA 94720, United States of America

E-mail: mesbah@berkeley.edu

Received 15 March 2017, revised 7 June 2017
Accepted for publication 28 June 2017
Published 26 July 2017

Abstract

Atmospheric pressure plasma jets (APPJs) have been identified as a promising tool for plasma medicine. This paper aims to demonstrate the importance of using model-based feedback control strategies for safe, reproducible, and therapeutically effective application of APPJs for dose delivery to a target substrate. Key challenges in model-based control of APPJs arise from: (i) the multivariable, nonlinear nature of system dynamics, (ii) the need for constraining the system operation within an operating region that ensures safe plasma treatment, and (iii) the cumulative, nondecreasing nature of dose metrics. To systematically address these challenges, we propose a model predictive control (MPC) strategy for real-time feedback control of a radio-frequency APPJ in argon. To this end, a lumped-parameter, physics-based model is developed for describing the jet dynamics. Cumulative dose metrics are defined for quantifying the thermal and nonthermal energy effects of the plasma on substrate. The closed-loop performance of the MPC strategy is compared to that of a basic proportional-integral control system. Simulation results indicate that the MPC stategy provides a versatile framework for dose delivery in the presence of disturbances, while the safety and practical constraints of the APPJ operation can be systematically handled. Model-based feedback control strategies can lead to unprecedented opportunities for effective dose delivery in plasma medicine.

Keywords: atmospheric pressure plasmas, feedback control, plasma medicine, dose delivery, model predictive control

1. Introduction

Cold atmospheric plasmas (CAPs) comprise a set of relatively new plasma sources that allow treatment of heat and pressure sensitive substrates [1]. Over the past decade, CAPs have found applications in etching, functionalization, and surface activation of sensitive polymeric materials such as biopolymers [2, 3]. CAPs have also been used for therapeutic treatment in plasma medicine [4]. In addition to their well-established bactericidal effects [5, 6], it has been demonstrated that CAPs can lead to reduction in tumor size and pain relief in cancer patients [7], enhanced healing of chronic wounds [8], and control of multidrug resistant bacteria [9].

Plasma medicine generally aims to evoke a combination of effects on a target substrate [4]. *In vivo* experiments have elucidated that plasma effects on biological substrates are highly nonlinear and cumulative (e.g. [10, 11]). The cumulative (i.e., time-integral, nondecreasing) nature of plasma effects implies that these effects are 'nonretractable', that is, once they are delivered to a substrate the effects cannot be removed [12, 13]. In addition, multiple plasma effects can act synergistically, augmenting the observed impact on the substrate. For example, mild thermal stress on tissues can affect their susceptibility to other mechanisms of cellular deactivation, including the up-regulation of intracelluar reactive oxygen and nitrogen species (RONs) generation [14]. Thus, the notion of *dose delivery* in plasma medicine critically hinges on quantifying the cumulative, nonlinear nature of

[1] Author to whom any correspondence should be addressed.

multiple plasma effects on a substrate. In the absence of cumulative dose metrics, however, the common practice has been to use the plasma treatment time under some prescribed protocol as a proxy for the cumulative plasma effects [15]. This approach can be inadequate for capturing the complexity of dose delivery in CAP treatments due to the variability in characteristics of the plasma and target substrate as well as the sensitivity of a plasma treatment to operating conditions and disturbances.

While plasma dose definition and quantification in a medical sense is beyond the scope of this work, the goal of this paper is to present a model-based feedback control strategy for safe, reproducible, and effective dose delivery in plasma medicine. To this end, we use an atmospheric pressure plasma jet (APPJ) as a model CAP system. APPJs have gained increasing attention due to their operational flexibility and versatile discharge chemistry [16]. In APPJs, ring and rod (or needle) electrodes are configured in and around a dielectric tube, which directs the flow of a carrier gas (typically helium or argon) and serves as a dielectric barrier [17]. The gas flow (typically $\sim$1–5 slm) allows the visible plasma plume to extend up to several centimeters beyond the tip of the dielectric tube, allowing for flexibility in surface treatment. Small admixtures of molecular gasses (e.g. oxygen, air, or water vapor) are commonly introduced to the gas flow to enhance the discharge chemistry [18]. In direct plasma treatment, the APPJ is electrically coupled to the target substrate [17]. Direct plasma treatment allows generation of chemically active species close to the target substrate and, therefore, can enhance the plasma effects [19]. However, direct treatment can lead to an intricate interplay between the plasma and substrate properties [20, 21]. Application of APPJs for plasma medicine often requires translation of the device over a surface area of the substrate such as human skin, wounds or tumors, which may have varying properties. Unmeasured properties of the substrate such as roughness, charge, electrical impedance, and water content can act as system disturbances influencing the plasma treatment. In addition, the inter-electrode distance (i.e., distance between the tip of the jet and substrate) in direct plasma treatment may vary uncontrollably in hand-held applications of APPJs, leading to different effects across the target substrate. This is due to the fact that APPJs typically exhibit steep spatial gradients over the inter-electrode distance to an extent that concentration gradients of reactive species and gas temperature can be, respectively, on the order of 10^{15} cm^{-3}/cm and 10 K cm^{-1}along the plasma plume [22]. Consequently, the plasma stability [23] as well as the observed plasma effects on the substrate, such as cell death [15], can change drastically due to even minor variations in the inter-electrode distance.

The resulting variability in APPJ operation due to the above described disturbances can severely hamper safe, reproducible, and effective dose delivery in plasma medicine. This paper presents an optimization-based feedback control method, known as model predictive control (MPC) [24, 25], for safe (e.g. arc-free) and systematic dose delivery using APPJs while ensuring safe operation of the jet (e.g. arc-free) in the presence of disturbances. MPC seeks to optimize the APPJ performance for multicomponent dose delivery based on the knowledge of the jet dynamics, described by a mathematical model, and system constraints. MPC can explicitly account for the nonlinear (often cumulative) nature of plasma dose mechanisms and systematically trade-off between multiple (possibly conflicting) dose delivery mechanisms. In addition, the inclusion of system constraints into MPC will allow for restricting the APPJ operation within a predetermined operating range to ensure safe and reproducible dose delivery. In this paper, we demonstrate the MPC strategy for feedback control of a radio-frequency (RF) APPJ in pure argon as a model system. To address the computational requirements of online optimization in MPC, a physics-based, lumped-parameter model is developed for the APPJ under study, which describes the electrical properties of plasma as well as the mass and heat transfer along the gas plume. Provisional dose metrics are defined to quantify the thermal and nonthermal energy effects delivered to a target substrate. The closed-loop performance of MPC is compared to that of a basic proportional-integral (PI) control system, which is designed using the internal model control (IMC) method [26]. Two simulation case studies are considered: (i) rejection of variations in the inter-electrode distance in direct APPJ treatment, and (ii) multicomponent dose delivery. Even though model-based control of other plasma applications (e.g. plasma etch processes [27–29] and tokamak reactors [30–32]) has been investigated in the past, to the best of authors' knowledge, this work is the first investigation on model-based feedback control for CAPs.

2. Model-based feedback control for APPJs

APPJs exhibit highly nonlinear, spatially distributed dynamics, with characteristic times that vary over several orders of magnitude [33]. The dynamics of electron impact reactions in the plasma and the dynamics of heat and mass transport processes along the jet occur on the timescales of nanoseconds and milliseconds to seconds, respectively, while treatment times in typical medical APPJ applications can take up to several minutes [5, 6]. In addition, the dynamics of APPJs are multivariable. That is, APPJs often have several input variables (e.g. amplitude and frequency of the applied voltage, flow rate and composition of the inlet gas) that can be modulated to induce several plasma effects such as electric field, heat, UV photons, and RONs that interact with the target substrate and with each other. The nonlinear couplings between the various input variables and the multiple plasma effects can make it impractical to achieve the desired plasma effects via independently modulating the jet inputs.

Another key consideration in feedback control of APPJs is to effectively constrain the jet operation within an operating range that prevents mode transitions and development of instabilities in the plasma. In RF-APPJs, for example, the voltage–current (V–I) operating range that corresponds to a 'normal glow' mode often spans over a relatively narrow range of currents [16]. Thus, the plasma is susceptible to instabilities and transition to arc or spark when small changes

in electrical properties occur. Distinct modes have been reported for RF-APPJs, where mode transitions can occur via the sheath breakdown events associated with secondary electron emission from the electrode surface [34–36]. Mode transitions can lead to high current densities and negative differential conductivity, resulting in instabilities and arc-like behavior that can inflict damage on the target substrate [37, 38]. In medical APPJ applications, it is imperative to ensure stable and reproducible operation of the APPJ through preventing undesired mode transitions in the plasma.

The multivariable, nonlinear dynamics of APPJs, the necessity of constraining the plasma operation within a prespecified region, and the cumulative and likely multicomponent nature of plasma dose metrics comprise some of the key challenges in feedback control of APPJs. Conventional proportional-integral-derivative (PID) controllers [39] cannot systematically address these challenges. This is because PID control systems are designed based on linear, single-input–single-output descriptions of system dynamics, thus disregarding the complex nature of APPJ dynamics due to nonlinear couplings between various jet inputs and plasma effects. In addition, PID controllers cannot handle constraints on system variables, while effective handling of constraints, for example, on plasma current and gas temperature is paramount for ensuring safe operation of the jet. This paper considers the MPC approach to feedback control of APPJs. The conceptual simplicity of MPC as well as its ability to systematically handle the complex (i.e., nonlinear and multivariable) dynamics of APPJs, constraints on input and system variables, and multicomponent dose metrics make MPC a suitable strategy for feedback control of APPJs in biomedical applications. In the remainder of this paper, the key features of MPC will be demonstrated for a model RF-APPJ in pure argon.

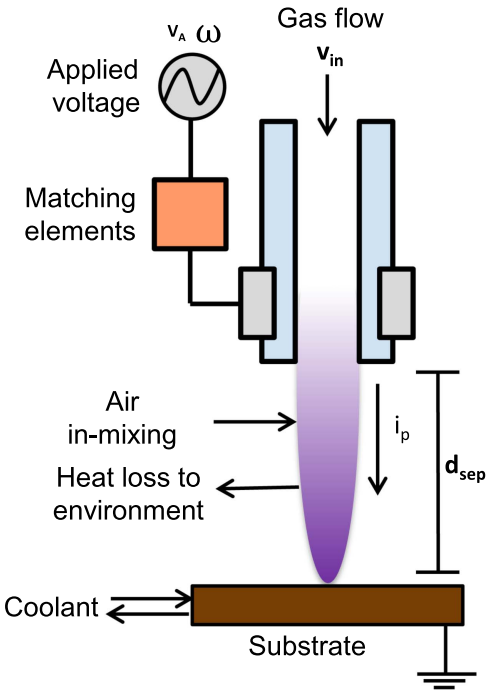

Figure 1. Schematic of the RF-APPJ in pure argon. Ar flows through a dielectric tube, entering the tube at velocity v_{in} and is excited to form a plasma by an RF voltage V_A applied via a matching network to an external electrode ring at frequency ω. Current i_p passes through the plasma plume to the substrate. The substrate, in general, has a complex electrical impedance Z_s, coupling the plasma current in the jet to ground. The tube tip is within a distance d_{sep} from the grounded, cooled substrate. Air components and heat are exchanged radially between the Ar jet and the surrounding air.

3. The model system: RF-APPJ in argon

This section describes a RF-APPJ in argon, which is used as a model system for demonstrating the concept of MPC. Since MPC involves solving a generally complex optimization problem in real-time, the system model used in MPC must be as simple as practicable. A relatively simple physics-based, lumped-parameter model is presented for the RF-APPJ, which will be used for designing the MPC controller in section 4. To evaluate the performance of the MPC controller for dose delivery, provisional dose metrics are proposed for quantifying the thermal and nonthermal energy effects of plasma on a substrate. The dose metrics will be explicitly used in the formulation of the MPC controller. It should be stressed that although the provisional dose definitions used in this paper are not necessarily the ones that will ultimately be used in a medical setting, they share the key properties of being both cumulative and nonlinear. We suggest that being able to safely achieve cumulative dose delivery is a necessary characteristic of a control system for plasma medicine, but we acknowledge that there may be other factors that may be important in future applications that we have not yet anticipated.

3.1. System description

A schematic representation of the APPJ under study is shown in figure 1. The APPJ is an RF-excited pure argon (Ar) plasma, with no additional gas admixing in the inlet. The RF-APPJ is used for direct treatment—there is no separate ground electrode on the dielectric tube. Thus, the plasma extends as a free jet, electrically coupled to surroundings and the target substrate (i.e., plasma current reaches the target substrate). The characteristics of the model jet are consistent with devices used in clinical APPJ applications (e.g. kINPen, INP Greifswald [8]). Details of the jet properties and operating conditions used in this paper are listed in appendix B. The considered APPJ configuration has been extensively investigated for biomedical applications [20, 35, 40], and has been the subject of several modeling studies [21, 41, 42]. A key challenge in using APPJs for direct plasma treatment (as in figure 1) arises from the high sensitivity of the electrical and thermal characteristics of the plasma jet to variations in the separation distance between the substrate and device [40], as well as variations in the electrical properties of the substrate [20, 21].

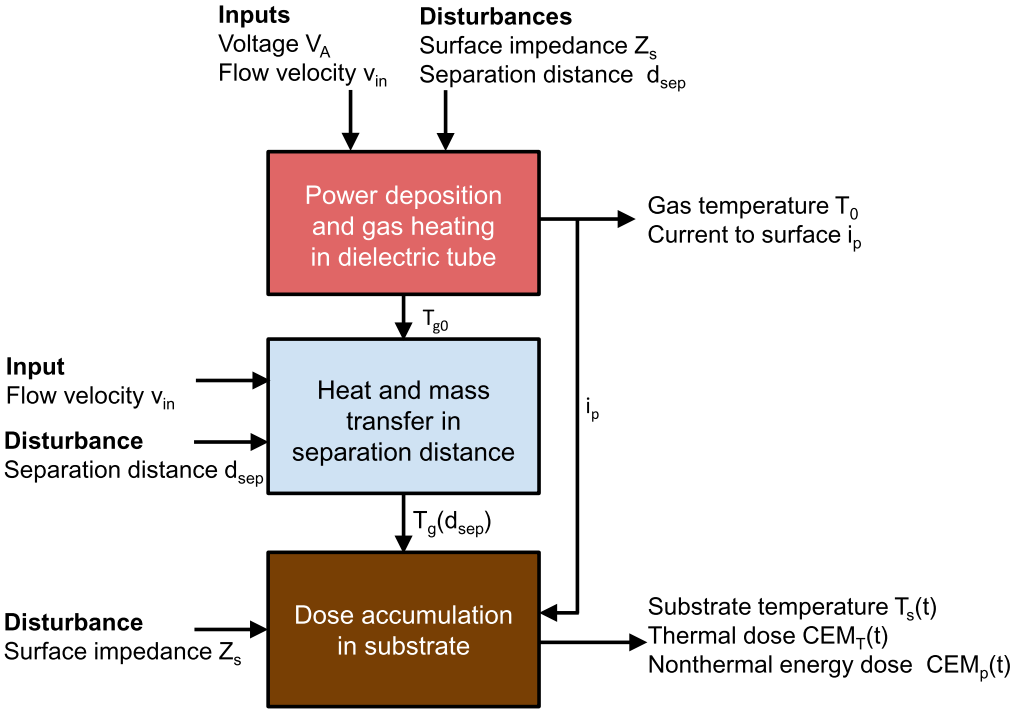

Figure 2. Framework of the physics-based model for the RF-APPJ coupled with a substrate. Input variables include applied voltage V_A and gas flow velocity v_{in} with disturbances associated with substrate impedance Z_s and tube tip-to-substrate separation distance d_{sep}. The model consists of three coupled modules: power deposition and gas heating in the dielectric tube (top), heat and mass transfer along the plasma plume (middle) and dose accumulation and substrate effects (bottom).

3.2. Physics-based, lumped-parameter modeling of the RF-APPJ

The principle of timescale separation is used to develop a lumped-parameter model for the RF-APPJ. Figure 2 depicts the modeling framework, which consists of three coupled modules—power deposition and gas heating within the dielectric tube, heat and mass transfer along the separation distance between the tip of the tube and the substrate, and dose accumulation in the substrate. The electrical power deposition in the plasma and the associated heating of the flowing Ar gas are assumed to occur adjacent to the ring electrode in the dielectric tube. The dynamics of power deposition and gas heating are neglected, implying that this module of the model is treated to be at steady state. The spatial variations within the dielectric tube are also neglected in order to obtain a zero-dimensional equivalent circuit model for the plasma. Under these assumptions, the plasma electrical properties can be described using a parametric expression of the complex plasma impedance in terms of plasma current, developed through analogy with a 1D RF parallel-plate discharge model [43]. This is described in greater detail in appendix A. The parametric expression of the complex plasma impedance is intended to capture aspects of the nonlinear behavior of the plasma electrical properties associated with the α–γ mode transition. Note that the Ar gas heating in the dielectric tube is coupled with the plasma electrical properties. This is due to the dependence of the plasma resistance on the gas number density (see appendix A.1). Modeling the RF jet plasma as a 0–D system inevitably introduces several approximations. Our goal, however, is to develop a plasma model that is computationally efficient and sufficiently accurate for the plasma process control application. We acknowledge that the proposed model must be validated in future experimental studies with practical devices.

The radial mixing of air and heat transfer along the free jet region between the tip of the tube and the substrate are approximated by lumped mass and heat transfer coefficients, respectively. The latter coefficients are obtained from a separate 2D axisymmetric COMSOL fluid model of mass and heat transfer in the distance between the tip of the tube and the substrate[2]. The length of the plume is assumed equivalent to the separation distance between the tube tip and the substrate (d_{sep} in figure 1). We note that this distance can change during hand-held operation of the APPJ. Since variations in the gas temperature and composition can depend strongly on the separation distance d_{sep}, the spatial distribution of gas temperature and composition along the flow axis is accounted for in the lumped-parameter model, as described in section 3.2.2. However, the dynamics of the transport phenomena along the separation distance are neglected.

The system model also includes the thermal and electrical effects of the plasma on the target substrate. The heat transfer coefficient between the incident jet and the substrate is obtained from the 2D axisymmetric COMSOL fluid model, assuming that the substrate properties are radially averaged. The accumulation of thermal and nonthermal energy effects

[2] For brevity, the details of these calculations are not described in this paper.

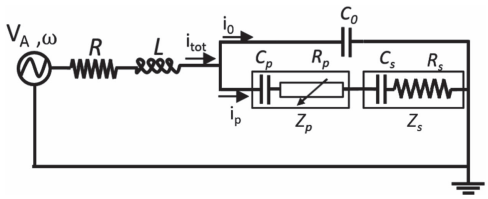

Figure 3. Equivalent circuit for the RF-APPJ [20]. See text for details.

of the plasma on the substrate is quantified using time-integral dose metrics. Note that the dynamics of dose accumulation on the substrate are significantly slower than the plasma dynamics within the dielectric tube and the heat and mass transfer dynamics along the separation distance. In the following, the physics-based model equations are presented.

3.2.1. Power deposition and gas heating in the dielectric tube. Figure 3 shows an equivalent circuit for the RF-APPJ, where R is the external circuit resistance, L is the matching inductance, C_0 is the parasitic capacitance, Z_p is the plasma complex impedance consisting of the bulk plasma resistance R_p and plasma capacitance C_p, and Z_s is the surface impedance with the resistive and capacitative components C_s and R_s, respectively. At steady state, the equivalent circuit can be modeled by Kirchhoff's second law

$$V_A - |Z_{\mathrm{ip}}| i_p = 0, \tag{1}$$

where the overall impedance Z_{ip} relates the plasma current i_p to the applied voltage V_A. The expression for Z_{ip} can be derived from the circuit structure (see appendix A.2).

The plasma impedance Z_p is a function of the plasma current i_p, gas temperature T_{g0}, and separation distance d_{sep}. As discussed in appendix A.1, this work adopts the following plasma resistance-current parameterization

$$R_p(i_p) = (-\alpha i_p + \beta)\frac{d_{\mathrm{sep}}}{T_{g0}}, \tag{2}$$

where the parameters α and β are estimated using predictions of a 1D model of a parallel-plate RF discharge in Ar [43]. The characteristic V–I behavior of the parameterization (2) is shown in figure A1 (appendix A.1). The peak in the V–I characteristic curve can be related to plasma stability. The differential plasma conductivity $(\mathrm{d}I/\mathrm{d}V)$ becomes negative when plasma current surpasses the peak value. This can result in a mode transition in the plasma [38]. Needle and ring-electrode APPJs can also exhibit similar characteristic V–I behavior [35, 44].

To determine the gas temperature T_{g0} in (2), a volume-averaged, steady-state energy balance is formulated for the gas in the dielectric tube region

$$\rho_{\mathrm{in}} v_{\mathrm{in}} c_{p\mathrm{Ar}} A_c (T_{\mathrm{in}} - T_{g0}) + \eta P = 0, \tag{3}$$

where T_{in}, ρ_{in}, and v_{in} are the inlet gas temperature, density, and velocity, respectively, $c_{p\mathrm{Ar}}$ is the specific heat capacity of argon, A_c is the cross-sectional area of the tube, η is an efficiency factor for the gas heating through power deposition into the neutral gas, and P is the total electrical power deposited in the plasma. The total power P is given by

$$P = \frac{1}{2}|i_p|^2 |Z_p| \cos(\phi), \tag{4}$$

where ϕ is the angle between the sinusoidal plasma current and applied potential. In the energy balance (3), the heat loss to the dielectric tube is neglected. Note that the total mass flow through the tube is equal to the product of gas density and velocity. Even though ρ and v vary with the gas temperature, the mass flow is constant and is equal to $\rho_{\mathrm{in}} v_{\mathrm{in}}$. Equations (1)–(4) constitute the equivalent circuit model in the dielectric tube, the parameters of which are given in table B1.

3.2.2. Heat and mass transfer along the separation distance between tube and substrate. As the gas plume extends to the substrate, it undergoes heat and mass transfer with surrounding air due to radial heat loss and in-mixing of air. The transport processes along the tip of the tube and substrate are described by a set of steady-state 1D mass and energy balances for a two-component system consisting of Ar and air. The steady-state energy balance along the gas flow axis is given by

$$\frac{\mathrm{d}T_g}{\mathrm{d}z} = -\frac{1}{\rho v c_p}\left(\frac{U}{r}(T_g - T_{\mathrm{inf}})\right), \qquad T_g(0) = T_{g0}, \tag{5}$$

where $T_g(z)$ is the gas temperature along the flow axis z, U is the lumped (radial) heat transfer coefficient across the plume radius r, T_{inf} is the ambient air temperature, and ρ, v, and c_p are the density, velocity, and heat capacity of the gas plume, respectively. Since it is assumed that no mass transfer occurs along the flow axis, the continuity equation yields $\rho v = \rho_{\mathrm{in}} v_{\mathrm{in}}$ (see appendix A.3). The gas temperature in the dielectric tube is used as the initial value for (5).

The gas density ρ is a function of gas composition, which in turn depends on the average molecular weight of the gas that flows between the tip of the tube and the substrate. This is obtained from a steady-state mass balance for Ar

$$\frac{\mathrm{d}m_{\mathrm{Ar}}}{\mathrm{d}z} = -\frac{P_{\mathrm{atm}}}{R\rho_{\mathrm{in}} v_{\mathrm{in}}}\frac{1}{T_g}(\mathrm{Mw}_{\mathrm{Ar}} m_{\mathrm{Ar}} + \mathrm{Mw}_{\mathrm{Air}}(1 - m_{\mathrm{Ar}})) \times \frac{k}{r}(m_{\mathrm{Ar}} - m_{\mathrm{inf}}), \qquad m_{\mathrm{Ar}}(0) = 1, \tag{6}$$

where $m_{\mathrm{Ar}}(z)$ is the Ar mass fraction along the flow axis z, P_{atm} is atmospheric pressure, R is the ideal gas constant, $\mathrm{Mw}_{\mathrm{Ar}}$ and $\mathrm{Mw}_{\mathrm{Air}}$ are the molecular weights of Ar and air, respectively, k is the lumped (radial) mass transfer coefficient, and $m_{\mathrm{inf}} = 0$ is the argon mass fraction in ambient air; see appendix A.3 for the derivation of (6). The lumped transport coefficients U and k in (5) and (6) are assumed to scale with the square root of the inlet argon velocity $\sqrt{v_{\mathrm{in}}}$ since the gas flow is in laminar or near-laminar regime. Model parameters are given in table B2. Note that the spatial integration bounds for (5) and (6) are set to $z = 0$ and $z = d_{\mathrm{sep}}$. Thus, the heat and mass transfer along the gas plume is dependent on the separation distance between the tip of the dielectric tube and substrate. When the air in-mixing along the gas plume is neglected, (5) can be solved analytically [45].

3.2.3. Dose accumulation in the substrate. We propose two provisional dose metrics for quantifying the *thermal* and *nonthermal* energy effects of plasma on a substrate. This section describes expressions for the dose metrics. A thermal dose is straightforward to understand—tissue heating has known effects for which equivalent thermal dose expressions have been proposed in the biomedical literature. We utilize an established expression to quantify the thermal effects of plasma. On the other hand, nonthermal energy dose in a plasma biomedical context can be related, for example, to fluxes of reactive chemical species, or possibly to effects associated with electrical charge or pulsed electric fields. To maintain generality in this paper, we propose a relatively simple dose metric for the nonthermal energy effects that is analogous to the thermal dose metric. The key feature of both expressions is that they are cumulative.

The thermal dose metric is defined in terms of the substrate temperature. The substrate is considered to be continuously cooled from below. In a biomedical context, this cooling would be provided by blood flow. Assuming that there exists no temperature gradients within the substrate, the dynamics of the substrate temperature $T_s(t)$ can be described by the Pennes' bioheat equation [46]

$$\frac{\mathrm{d}T_s}{\mathrm{d}t} = -\frac{\lambda_b c_b}{\rho_s c_{ps}}(T_s - T_b) + \frac{h}{\rho_s c_{ps} d_s}(T_g(d_{\mathrm{sep}}) - T_s) + \frac{0.5 i_p^2 R_s}{A_c \rho_s c_{ps} d_s}, \qquad T_s(0) = 311\ \mathrm{K}, \tag{7}$$

where d_s is the thickness of the substrate, λ_b, T_b, and c_b are the perfusion rate, temperature, and specific heat capacity of the coolant, respectively, ρ_s and c_{ps} are the density and specific heat capacity of the substrate, respectively, h is the heat transfer coefficient between the gas plume and the substrate, and $T_g(d_{\mathrm{sep}})$ is the gas plume temperature adjacent to the substrate. The last term in the right-hand side of (7) accounts for ohmic heating of the substrate due to the plasma current i_p. Model parameters are given in table B3.

To quantify thermal accumulation in the substrate, we adopt the *cumulative equivalent minutes* (CEM_T) metric, which is commonly used for thermal dose quantification in hyperthermia treatment [47]. The dose metric CEM_T is based on Arrhenius-type dependence of cell death on medium temperature [12], which has also been reported for cell death upon plasma treatment [15]. In this work, CEM_T is used to quantify the equivalent cumulative effect of substrate heating at the reference temperature 43 °C (in the unit of time, minutes). The latter reference temperature is commonly used in hyperthermia treatment [12]. The dose metric CEM_T is defined by

$$\mathrm{CEM}_T = \int_0^t K^{(43 - T_s(\tau))}\,\mathrm{d}\tau \tag{8}$$

or, equivalently,

$$\frac{\mathrm{dCEM}_T}{\mathrm{d}t} = K^{(43 - T_s(t))}, \qquad \mathrm{CEM}_T(0) = 0, \tag{9}$$

where the constant K is given by

$$K = \begin{cases} 0 & T_s \leqslant 39\ ^\circ\mathrm{C} \\ 0.25 & 39\ ^\circ\mathrm{C} < T_s < 43\ ^\circ\mathrm{C} \\ 0.5 & T_s \geqslant 43\ ^\circ\mathrm{C}. \end{cases} \tag{10}$$

CEM_T is a cumulative, time-integral metric, which implies that the thermal dose delivered to the substrate cannot be removed. To illustrate the qualitative behavior of CEM_T, figure 4(a) shows the equivalent thermal accumulation at the reference temperature 43 °C over a treatment time of 1 min as a function of the substrate temperature. Figure 4(a) suggests that 1 °C increase in the substrate temperature when T_s is greater than the reference temperature requires shortening the treatment time by half in order to achieve the same effective thermal accumulation in the substrate. A key feature of CEM_T is that it captures the effects of both the treatment time and the treatment temperature.

Similarly, a CEM metric at a reference energy flux is defined to quantify the accumulation of nonthermal energy effects of the gas plume in the substrate. The dose metric CEM_P quantifies the lumped, nonthermal energy absorbed by the substrate, for example, in the form of chemical energy due to reactive species and/or possibly other energy forms (in the unit of minutes at energy flux). In this work, the nonthermal energy delivered to the substrate is due to the remnant of the total plasma power that has not been deposited in the dielectric tube for gas heating. The nonthermal energy is denoted by $\bar{P} = (1 - \eta)P$ (note the efficiency factor $\eta < 1$ in (3)). The nonthermal energy dose metric CEM_P is defined by

$$\mathrm{CEM}_P = \int_0^t \gamma \frac{\bar{P}(\tau)}{A_c}\mathrm{d}\tau \tag{11}$$

or, equivalently,

$$\frac{\mathrm{dCEM}_P}{\mathrm{d}t} = \gamma \frac{\bar{P}(t)}{A_c}, \qquad \mathrm{CEM}_P(0) = 0, \tag{12}$$

where γ is an absorption coefficient for the efficacy of the nonthermal energy transfer from the gas plume to the substrate. In (12), the constant γ takes the value 0.2 $\mathrm{cm^2\ W^{-1}}$, which corresponds to a reference nonthermal energy flux of 75 $\mathrm{J\ cm^{-2}\ min^{-1}}$ (i.e., CEM_P equals 1 for the delivery of 75 $\mathrm{J\ cm^{-2}}$ over 1 min). The time dependence of the plasma power $\bar{P}(t)$ arises from variations in the APPJ inputs (see (4)). The cumulative behavior of CEM_P is shown in figure 4(b). Note that while here CEM_P has the unit of minutes, it can also be expressed in the unit of total equivalent fluence ($\mathrm{J\ cm^{-2}}$).

We recognize that the chosen functional forms of the dose metrics (8) and (11) are somewhat arbitrary. However, these dose metrics can effectively describe the cumulative characteristic of various dose delivery mechanisms in medical applications of CAPs. In fact, *in vitro* and *in vivo* studies have shown that RONs typically exhibit a nonlinear, nondecreasing absorption behavior (e.g. [48, 49]), which can be captured by a dose metric of the form (8). On the other hand, the linear behavior of the dose metric (12) is analogous to assuming that the plasma effects are described by a constant absorption rate

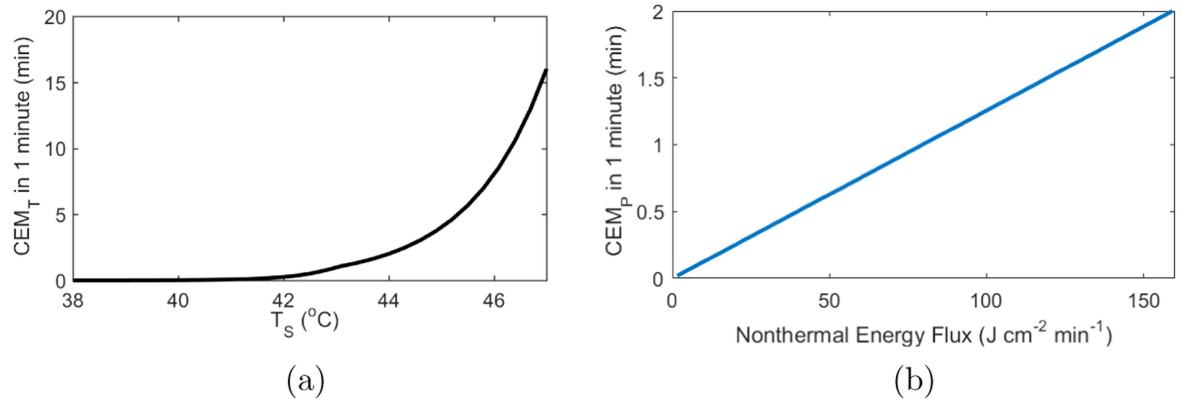

Figure 4. (a) Thermal energy accumulation CEM_P during one minute treatment as a function of the substrate temperature T_s; (b) nonthermal energy accumulation CEM_T during one minute treatment as a function of power deposited onto substrate per area. The dose metrics are nondecreasing and have a time unit in minutes.

(e.g. [50, 51]). The framework of the MPC strategy presented in section 4 for the feedback control of APPJs can be readily modified to accommodate user-defined dose metrics.

3.3. State-space representation of the lumped-parameter model

The physics-based, lumped-parameter model of the RF-APPJ with the target substrate is described by the set of nonlinear, differential algebraic equations (1)–(12); see figure 2. The system model can be compactly represented by a discrete-time, state-space description

$$\begin{aligned} x_{k+1} &= f(x_k, z_k, u_k, \theta), \qquad x_0 = x(0) \\ 0 &= g(x_k, z_k, u_k, \theta), \end{aligned} \tag{13}$$

where k is the time index, $x_k = [T_s\ \mathrm{CEM}_T\ \mathrm{CEM}_P]^\top$ is the vector of differential state variables with the initial conditions x_0, $z_k = [T_{g0}\ i_p\ P\ T_g(z)\ m_{\mathrm{Ar}}(z)]^\top$ is the vector of algebraic state variables, $u = [V_A\ v_{\mathrm{in}}]^\top$ is the vector of RF-APPJ inputs, θ is the vector of model parameters (given in appendix B), and f and g are the nonlinear differential and algebraic model equations, respectively. Variations in the separation distance between the tip of the tube and substrate (d_{sep}) are considered as an unmeasured system disturbance. In section 4, the nonlinear state-space model (13) is used for designing the MPC controller.

4. Feedback control strategies for RF-APPJ

This section describes the design of MPC and PI controllers for the feedback control of the RF-APPJ at hand. Two case studies are presented for comparing the performance of the MPC and PI controllers using closed-loop simulation studies.

4.1. Model predictive control

MPC is an optimization-based control method. The key notion of MPC is to optimize the predicted behavior of a system over a prediction horizon in terms of some user-specified performance criteria, while enforcing constraints on the system state and input variables [24, 25]. To incorporate measurement feedback into MPC, the online system information obtained at every measurement sampling time is used to initialize the underlying system model in MPC. This is known as *receding-horizon control*, which provides MPC with some degree of robustness to system uncertainties and unmeasured disturbances. The general mathematical formulation of an optimal control problem, solved recursively in MPC, is given in appendix C. A key consideration in any MPC design is the computational complexity of the system model, which must be amenable to online solution of the optimization problem.

MPC offers several advantages over PID control, which include the ability to directly handle the dynamics of nonlinear systems with multiple inputs and multiple outputs (i.e., multivariable dynamics), state and input constraints, and multiple (potentially conflicting) control objectives. MPC has shown exceptional success in a wide range of applications including robotics and path planning, aerospace and automotive applications, energy systems, and chemical processes (e.g. [52–55]). In this paper, two MPC controllers are designed for the RF-APPJ, as described in the following case studies.

Case study I (disturbance rejection): the goal of this case study is to maintain the substrate temperature T_s and the plasma power P at user-specified setpoints, while counter acting the effects of a step change in the separation distance d_{sep}. The control objective function in the optimization problem (C.1) is defined by

$$J = \sum_{i=0}^{N_P} (T_{s,i} - T_s^{\mathrm{ref}})^2 + w(P_i - P^{\mathrm{ref}})^2, \tag{14}$$

where N_P is the prediction horizon, $T_s^{\mathrm{ref}} = 315$ K and $P^{\mathrm{ref}} = 5$ W are the setpoints for the substrate temperature and plasma power, respectively, and w is a constant chosen such that both setpoint tracking objectives have an equal weight in the

objective function (14). The prediction and control horizons in the optimization problem (C.1) are chosen as 20 and 3, respectively (see appendix C). State constraints are defined to maintain the plasma current and power below critical values in order to avoid potentially damaging conditions (e.g. arcing) as well as to keep the substrate temperature within a comfort level. Accordingly, the state constraints are defined by

$$\begin{bmatrix} T_s \\ i_p \\ P \end{bmatrix} \leqslant \begin{bmatrix} 316\ \text{K} \\ 2.5\ \text{mA} \\ 10\ \text{W} \end{bmatrix}. \tag{15}$$

In addition, the APPJ input values must be maintained within the following bounds

$$\begin{bmatrix} 100\ \text{V} \\ 8\ \text{m s}^{-1} \end{bmatrix} \leqslant \begin{bmatrix} V_A \\ v_{\text{in}} \end{bmatrix} \leqslant \begin{bmatrix} 700\ \text{V} \\ 35\ \text{m s}^{-1} \end{bmatrix}, \tag{16}$$

where the lower input bounds correspond to the minimum input values required for sustaining the plasma and the upper input bounds correspond to the physical limitations of the APPJ. The rates of input change are also bounded as

$$\begin{bmatrix} \Delta V_A \\ \Delta v_{\text{in}} \end{bmatrix} \leqslant \begin{bmatrix} 300\ \text{V} \\ 13.5\ \text{m s}^{-1} \end{bmatrix}. \tag{17}$$

Case study II (dose delivery): the goal of this case study is to safely deliver prescribed thermal and nonthermal energy doses to the substrate within a given treatment time of 150 s, without inflicting damage on the substrate. The control objective function is formulated as

$$J = (\text{CEM}_{T,N_t} - \text{CEM}_T^{\text{ref}})^2 + w(\text{CEM}_{P,N_t} - \text{CEM}_P^{\text{ref}})^2, \tag{18}$$

where the time index N_t corresponds to the total treatment time 150 s, $\text{CEM}_T^{\text{ref}} = 9$ min and $\text{CEM}_P^{\text{ref}} = 3$ min (corresponding to an equivalent fluence of $225\ \text{J cm}^{-2}$) are the prescribed setpoints for the thermal and nonthermal energy doses, respectively, and w is a constant. The control objective function (18) implies that the dose delivery problem requires that the thermal and nonthermal energy dose accumulation reach its prescribed target at the end of the treatment time. To ensure safe dose delivery, not only the plasma current and power must be constrained to prevent mode transition, but also the dose accumulation CEM_T and CEM_P must remain below prescribed limits at all times to avoid inflicting damage on the substrate. Thus, the following state constraints are defined

$$\begin{bmatrix} T_s \\ i_p \\ P \\ \text{CEM}_T \\ \text{CEM}_P \end{bmatrix} \leqslant \begin{bmatrix} 319\ \text{K} \\ 3.7\ \text{mA} \\ 12\ \text{W} \\ 10\ \text{min} \\ 5\ \text{min} \end{bmatrix}. \tag{19}$$

The input bounds and the bounds on the rates of input change in this case study are defined as in (16) and (17). The interior-point optimization algorithm IPOPT [56] is used to solve the optimization problem (C.1) in both case studies. The closed-loop performance of the MPC controllers in Case Studies I and II is compared to that of a PI control system, as demonstrated in section 5.

4.2. Proportional-integral control

PI control is the simplest and most widely used feedback control method [39]. PI control is based on an error signal e, computed in terms of the difference between a measured system output and its user-specified setpoint. The error signal is used to determine a control action $u(t)$ that steers the system output to its setpoint. The control action is computed in terms of the instantaneous (proportional-action) and accumulated (integrating-action) error

$$u(t) = k_p\left(e(t) + \frac{1}{\tau_i}\int_0^t e(\tau)\mathrm{d}\tau\right), \tag{20}$$

where the proportional gain k_p and the integral-time constant τ_i are the tuning parameters of a PI controller. The PI controller (20) is linear, and relates only one system input to one system output. Thus, input-output pairing is necessary for PI control design when the system has multiple input and output variables, as in the case in the APPJ at hand.

In this work, sensitivity analysis is performed to assess the effect of each input on each output of the APPJ. Accordingly, the plasma power P is paired with the input voltage V_A and the substrate temperature T_s is paired with the inlet flow velocity v_{in}. Since the dynamics of power deposition and gas heating in the dielectric tube are fast, relative to the substrate and dose accumulation dynamics (see 3.2), a proportional-only controller (excluding the integrating action in (20)) is used for regulating the plasma power. To enable a consistent comparison with the MPC controllers described in section 4.1, the IMC method [26] is used for tuning of the PI controllers. To this end, the nonlinear state-space model (13) is used to characterize the first-order-plus-deadtime dynamics between the paired inputs and outputs. Thus, the same system model is used for designing the MPC and PI controllers. The tuning parameters of the PI controllers are given in table D1 in appendix D. *Antiwindup* [57] is incorporated into the PI controllers to handle the input bounds considered in the MPC controllers.

For Case Study I, the same setpoints as in the control objective function (14) are used to design the PI controllers. On the other hand, the dose metrics CEM_T and CEM_P used in Case Study II cannot be readily incorporated into the PI controllers due to their nondecreasing, cumulative nature. Thus, the target doses $\text{CEM}_T^{\text{ref}}$ and $\text{CEM}_P^{\text{ref}}$ in (18) are translated into, respectively, their corresponding substrate temperature setpoint $T_s^{\text{ref}} = 318$ K and plasma power setpoint $P^{\text{ref}} = 6$ W for the prescribed treatment time 150 s (see (8) and (11)). The latter setpoints are then used in the PI controllers for substrate temperature and plasma power setpoint tracking.

5. Closed-loop simulation results and discussion

The closed-loop control systems with the MPC controller and the PI controllers are shown in figure 5. In the closed-loop control simulation studies presented below, the nonlinear

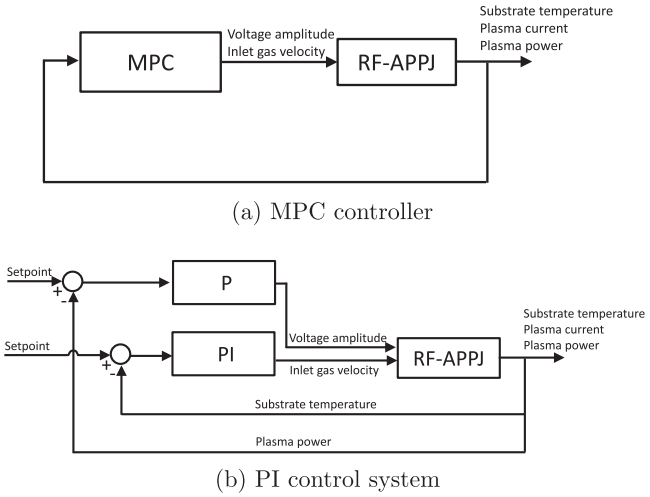

Figure 5. Block diagram of the closed-loop control systems for the RF-APPJ: (a) the MPC controller which uses measurements of substrate temperature, plasma current, and plasma power for manipulating applied voltage and inlet gas velocity, and (b) the PI control system which is designed to achieve the same control objectives using a single-input–single-output proportional controller and a proportional-integral controller.

state-space model (13) is used to represent the true system[3]. In all simulations, the measurement sampling time is 5 s.

Case study I (disturbance rejection): this case study is designed to assess the ability of the MPC controller and the PI control system to achieve setpoint tracking for the substrate temperature and plasma power while counteracting the effects of a step change in the separation distance between the tip of the tube and the substrate (i.e., d_{sep}). The separation distance undergoes a step change from 7.5 to 3 mm at time 50 s, as reported in the experimental study in [15]. The state constraints (15) are incorporated into the MPC controller to ensure that the plasma properties remain within some prespecified thresholds. This can be important when the plasma has a tendency to undergo a transition to a spark or some other undesirable mode.

The closed-loop simulation results are shown in figure 6. The step change in d_{sep} at 50 s results in an increase in the plasma current (figure 6(b)). The PI control system can effectively maintain the substrate temperature and plasma power at their respective setpoints after the step change in d_{sep} (figures 6(a) and (c)). However, the plasma current exceeds the specified current constraint of 2.5 mA. The PI controllers cannot handle state constraints to retain the jet operation within a desired operating region. This implies that the safe operation of the APPJ may be compromised when disturbances act on the APPJ (in this case, the step change in d_{sep}). The APPJ inputs (i.e., voltage amplitude and inlet gas velocity) computed by the PI controllers are shown in figures 6(d) and (e). The antiwindup property of the PI controllers enables retaining the inputs within their admissible bounds. However, the PI control system cannot systematically exploit the mutlivariable dynamics of the APPJ as the two PI controllers operate independently from each other.

On the other hand, MPC exploits the multivariable nature of the system dynamics for achieving the control objectives. The MPC controller simultaneously modulates both APPJ inputs V_A and v_{in} to achieve the setpoint tracking objective for the substrate temperature and plasma power (as defined in (14)). In comparison with the PI control system, the MPC controller leads to more effective setpoint tracking for substrate temperature until the separation distance is changed at 50 s (see figure 6(a)). After the step change in the separation distance, the performance of the MPC controller slightly degrades due to the offset in setpoint tracking for T_s and P. However, as shown in figure 6(b), the MPC controller can effectively fulfill the constraint on the plasma current in the presence of the step change in the separation distance (i.e., disturbance). The ability to handle state constraints is paramount for safe and reliable operation of the plasma jets, particularly in safety-critical applications such as in plasma medicine. State constraints can be motivated by various considerations for the safe operation of APPJs, such as avoiding plasma mode transitions via restricting the plasma state to a prespecified operating window, or accounting for requirements of the target substrate (e.g., a temperature range for comfortable treatment). Even though not demonstrated in this work, the slight offset in the setpoint tracking in figures 6(a) and (c) can be eliminated using standard offset-free MPC techniques [58]. The key advantage of MPC in this case study lies in its ability to realize multiple control objectives (setpoint tracking for T_s and P) while handling constraints on the system variables (constraint on i_p) and bounds on the system inputs (bounds on V_A and v_{in}).

Case study II (dose delivery): this case study aims to demonstrate the importance of using an advanced feedback control stategy, such as MPC, for safe and effective dose delivery. The objective is to deliver a target thermal dose CEM_T and nonthermal energy dose CEM_P to the substrate by the end of the treatment time 150 s. To avoid inflicting damage on the substrate, for example, due to undesired mode transitions or arcing, the plasma power and current are constrained in the MPC controller to remain below a certain threshold at all times during the APPJ operation (see (19)). In addition, upper constraints are imposed on CEM_T and CEM_P to prevent excessive dose delivery during the plasma treatment. The substrate temperature is constrained, for example, to ensure comfort of a patient being treated. Note that these state constraints cannot be handled in the PI control system.

The closed-loop simulation results for the MPC controller and the PI control system are shown in figure 7. As discussed in section 4.2, the PI controllers cannot readily accommodate the cumulative dose metrics (8) and (11). Consequently, the dose delivery problem for the PI controllers is defined in terms of setpoint tracking for the substrate temperature T_s and plasma power P, the setpoints of which were determined based on the target dose levels for CEM_T and CEM_P to be delivered over 150 s. Figures 7(d) and (e) indicate that the PI control system fails to safely realize the

[3] In closed-loop control simulation studies, the model used as the true system is typically different from that used in the controller.

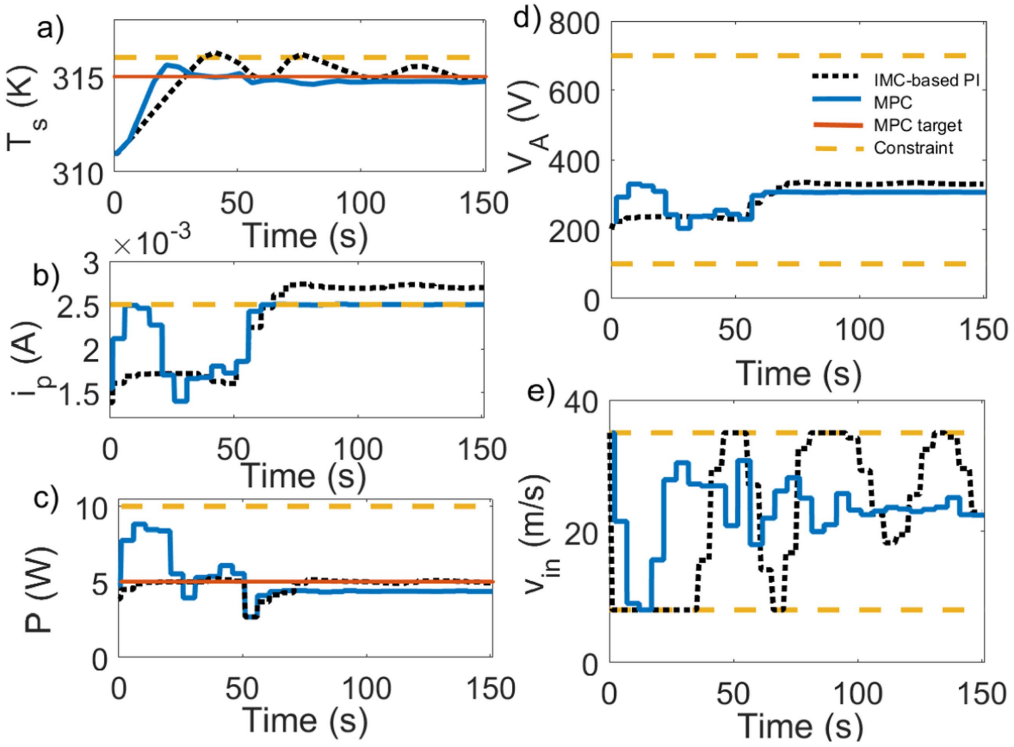

Figure 6. Closed-loop simulation results for the MPC controller and the PI control system in Case Study I: (a) substrate temperature, (b) plasma current, (c) plasma power, (d) voltage amplitude, and (e) inlet gas velocity.

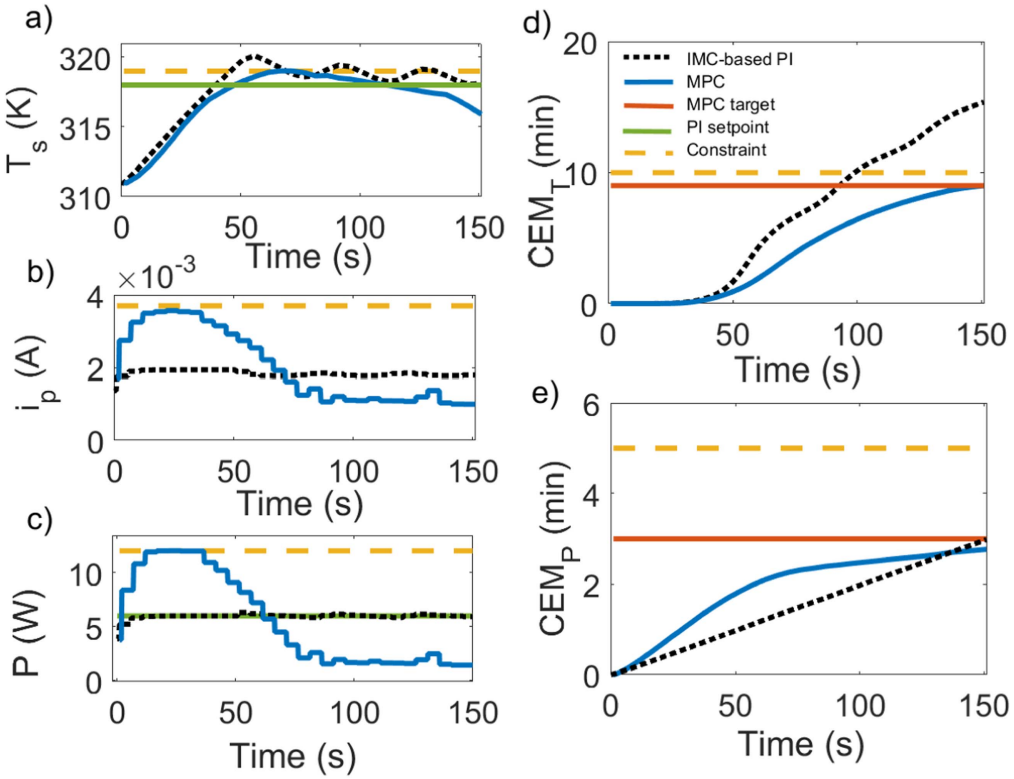

Figure 7. Closed-loop simulation results for the MPC controller and the PI control system in Case Study II: (a) substrate temperature, (b) plasma current, (c) plasma power, (d) thermal dose CEM_T, and (e) nonthermal energy dose CEM_P.

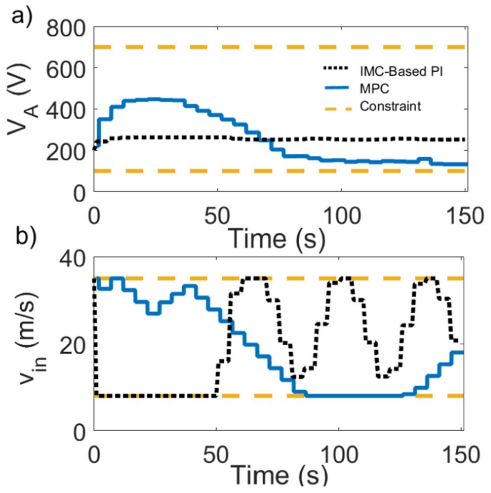

Figure 8. Input profiles computed by the MPC controller and the PI control system in Case Study II: (a) applied voltage and (b) inlet gas velocity.

dose delivery objective since the dose metric CEM_T exceeds its target level and constraint. While the nonthermal energy dose CEM_P is delivered in 150 s, the violation of the safety threshold on CEM_T can inflict severe thermal damage on the substrate. Figure 7(a) shows that the constraint on the substrate temperature is also violated when the PI control system is used for dose delivery.

On the other hand, figure 7 shows that the MPC controller can effectively achieve the dose targets at 150 s while satisfying the comfort and safety constraints on the substrate temperature, plasma current, and plasma power. In the MPC controller the target thermal and nonthermal energy doses are defined in the objective function (18). In fact, the target doses are defined as soft constraints, suggesting that their fulfillment is not guaranteed (in contrast to the safety constraints on the plasma and subtrate properties that are enforced at all times). Thus, a slight offset in the nonthermal dose CEM_P with respect to its target value is observed (less than 10%). It is worth noting that it may not be possible to deliver any arbitrary combination of thermal and nonthermal dose due to the tight coupling between the thermal and nonthermal dose delivery mechanisms. However, MPC enables achieving a trade-off between the two dose delivery mechanisms through selection of the weight constant w in (18).

This case study demonstrates that the promise of MPC for systematic regulation of multiple cumulative (in this case, linear and nonlinear) plasma dose delivery mechanisms. This is likely to be paramount in plasma medicine, particularly in light of the time-integral nature of the dose metrics. Note that dose delivery is an intrinsically 'integrating process' because once a part of the dose is delivered it cannot be removed from the substrate. MPC allows for seeking trade-offs between possibly (conflicting) dose delivery mechanisms in a systematic and transparent manner. In addition, the constraint handling ability of MPC (figures 7(a)–(c)) is crucial for ensuring safe and reliable operation of the APPJ since the plasma properties can be restricted to a prespecified operating range. The control input profiles computed by the MPC controller and the PI control system are shown in figure 8. The MPC and PI controllers result in different input profiles. However, both control strategies can effectively retain the control inputs within their bounds (see (16)), which were defined based on the physical limitations of the APPJ.

6. Conclusions and future work

This work demonstrates the potential promise of model-based feedback control strategies for safe and effective dose delivery in plasma medicine using APPJs, irrespective of how dose metrics are ultimately defined. The ability to systematically handle the multivariable dynamics of APPJs, safety and practicality constraints on system states, and multiple dose delivery objectives can make MPC a particularly suitable feedback control strategy for APPJ applications. Closed-loop simulation studies reveal that basic PI control systems can be inadequate for safe and therapeutically effective application of APPJs for dose delivery. By contrast, MPC provides a versatile control framework that can explicitly account for the safety and practicality constraints of APPJ operation, as well as the cumulative (likely nonlinear) nature of dose delivery mechanisms. Safe and repeatable operation of the plasma devices will be essential to their eventual successful implementation in medicine. Plasma medical devices might be promising candidates for robotic control in the future, and we envision that model-based feedback control strategies will be crucial to this end. Other novel applications of atmospheric-pressure plasmas, for example in materials processing, will also benefit from model-based feedback control strategies.

In future work, the proposed physics-based, lumped-parameter modeling framework and the MPC strategy will be experimentally validated. The modeling framework will be extended to include gas-phase chemistry of long-lived neutral and metastable species. This will enable quantifying the effects of plasma chemistry on the substrate in order to develop MPC controllers that can systematically regulate the likely synergistic thermal, electrical, chemical, and possibly other effects of atmospheric-pressure plasmas for plasma medicine.

Acknowledgments

The authors acknowledge partial support from the United States Department of Energy, Office of Fusion Science Plasma Science Center (SC0012500) and from the National Science Foundation (1415022).

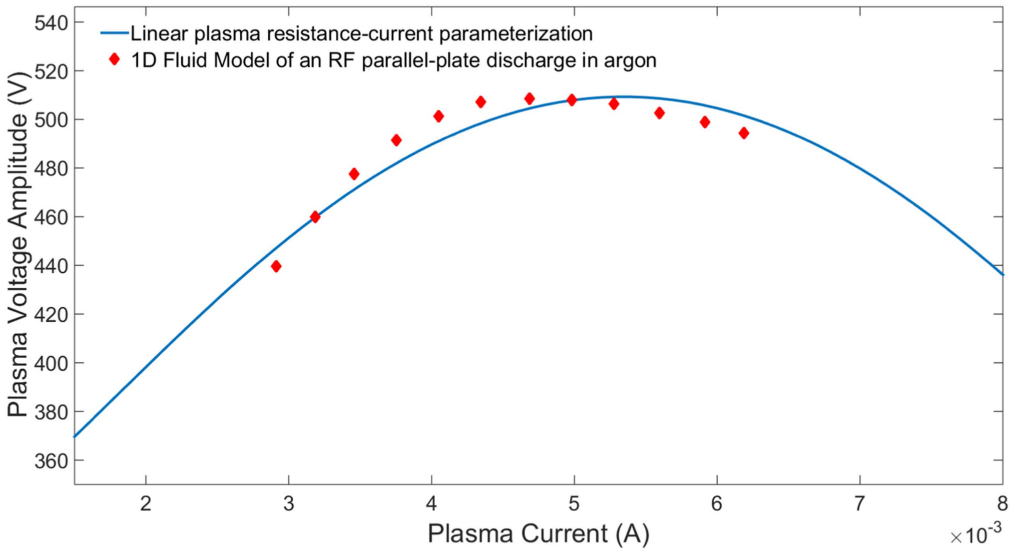

Figure A1. The voltage–current behavior predicted by the plasma resistance-current parameterization (2) and a 1D fluid model for an RF parallel-plate discharge in argon reported in [43]. Reproduced with permission from [43].

Appendix A. Lumped-parameter modeling of the RF-APPJ in argon

A.1. Parametrization of plasma resistance

The plasma resistance R_p can be described by [59]

$$R_p = \frac{V_p}{i_p} = \frac{d_{\text{sep}}}{S_e}\frac{m_e}{e^2}\frac{\bar{\nu}_{\text{eH}}}{n_e}, \tag{A.1}$$

where V_p is the plasma potential, i_p is the plasma current, S_e is the surface area of electrodes, m_e and e are the electron mass and charge, respectively, n_e is the electron density, and $\bar{\nu}_{\text{eH}}$ is the electron-heavy particle collision frequency. In direct plasma treatment, the inter-electrode distance in the RF-APPJ is equivalent to the separation distance between the tip of the dielectric tube and the substrate (d_{sep} in figure 1). Thus, the plasma resistance depends on the separation distance d_{sep}.

The plasma resistance is also dependent on the gas temperature through the electron-heavy particle collision frequency

$$\bar{\nu}_{\text{eH}} = K(T_e, n_e)n_0(T_{g0}), \tag{A.2}$$

where K is the collision rate constant that is a function of the electron temperature T_e and electron density n_e, n_0 is the neutral density, and T_{g0} is the gas temperature in the dielectric tube. The electron temperature T_e is assumed to be constant. This assumption is valid when a parallel-plate discharge is operated in the α mode [60]. In this mode, n_e can be assumed to vary linearly with the plasma current [60, 61], which yields the linear plasma resistance-current parameterization (2). Figure A1 shows the resulting *V–I* characteristic curve, which adequately describes the *V–I* behavior obtained from a 1D fluid model of a RF parallel-plate discharge in argon [43].

The dependence of the plasma resistance R_p on the gas temperature arises from the neutral density n_0, which is assumed to obey the ideal gas law

$$n_0 = \frac{P_{\text{atm}}}{k_{\text{b}}T_{g0}}, \tag{A.3}$$

where k_{b} is the Boltzmann constant and P_{atm} is atmospheric pressure. Notice that (A.2) and (A.3) indicate that the plasma resistance R_p is inversely related to the gas temperature T_{g0} in the dielectric tube.

A.2. Solution to the equivalent circuit model

In figure 3, the impedance Z_{ip}, which relates the plasma current i_p to the voltage amplitude V_A, is defined by

$$Z_{\text{ip}} = Z_p + Z_s + Z_c + Z_c\frac{(Z_p + Z_s)}{Z_0}, \tag{A.4}$$

where Z_c is the circuit impedance and Z_0 is the impedance associated with the parasitic capacitance C_0.

A.3. Velocity of the gas plume

For the separation distance between the tip of the dielectric tube and the substrate (d_{sep} in figure 1), the continuity equation can be written as

$$\frac{\text{d}(\rho v)}{\text{d}z} = 0, \qquad \rho v|_{z=0} = \rho_{\text{in}}v_{\text{in}}, \tag{A.5}$$

which implies that ρv is constant in the gas plume. The ideal gas law is used to obtain the average gas density ρ as a function of the gas temperature along the flow axis

$$\rho(z) = \frac{P_{\text{atm}}}{R}\frac{1}{T_g(z)}(\text{Mw}_{\text{Ar}}m_{\text{Ar}} + \text{Mw}_{\text{Air}}(1 - m_{\text{Ar}})). \tag{A.6}$$

From (A.5) and (A.6), the velocity of the plume gas is given by

$$v(z) = \rho_{\text{in}} v_{\text{in}} \frac{R}{P_{\text{atm}}} \frac{T_g(z)}{(\text{Mw}_{\text{Ar}} m_{\text{Ar}} + \text{Mw}_{\text{Air}}(1 - m_{\text{Ar}}))}. \quad \text{(A.7)}$$

Expression (6) is obtained by inserting (A.7) into the 1D continuity equation for Ar.

Appendix B. Model parameters

Table B1. Parameter values of the equivalent circuit model.

Parameter	Value
ω	13.56 MHz
R	50 Ω
L	1.04×10^5 H
C_0	0.1 μF
C_p	0.14 nF
α	-9.0×10^9 Ω K A^{-1} mm^{-1}
β	9.6×10^7 Ω K mm^{-1}
C_s	11.7 nF
R_s	100 Ω
η	0.5
$c_{p\text{Ar}}$	521.5 J kg^{-1} K^{-1}
ρ_{in}	1.63 kg m^{-3}

Table B2. Parameter values of the heat and mass transfer model.

Parameter	Value
U	$100\sqrt{v_{\text{in}}}$ W m^{-2} K^{-1}
k	$0.1\sqrt{v_{\text{in}}}$ m^2 s^{-1}
T_{inf}	298 K
r	1 mm
Mw_{Ar}	40 $gmol^{-1}$
Mw_{Air}	29 $gmol^{-1}$

Table B3. Parameter values of the substrate temperature model.

Parameter	Value
d_s	5 mm
λ_b	1 kg m^{-3} s^{-1}
T_b	310 K
c_b	3650 J kg^{-1} K^{-1}
c_{ps}	3680 J kg^{-1} K^{-1}
ρ_s	1020 kg m^{-3}
h	$36\sqrt{v_{\text{in}}}$ W m^{-2} K^{-1}

Appendix C. Formulation of the optimal control problem in MPC

MPC involves solving an optimal control problem at every time instant k that the system states x_k are measured [25]

$$\min_{\mathbf{u}} J(x_k, \mathbf{u})$$

$$\text{subject to:} \quad \bar{x}_{i+1} = f(\bar{x}_i, \bar{z}_i, u_i, \theta), \quad i = 0,\ldots, N_p - 1, \quad \text{(C.1}a\text{)}$$

$$0 = g(\bar{x}_i, \bar{z}_i, u_i, \theta), \quad i = 0,\ldots, N_p, \quad \text{(C.1}b\text{)}$$

$$l(\bar{x}_i, u_i, \bar{z}_i, \theta) \leqslant 0, \quad i = 1,\ldots, N_p, \quad \text{(C.1}c\text{)}$$

$$u_i \in \mathcal{U}, \quad i = 0,\ldots, N_c - 1, \quad \text{(C.1}d\text{)}$$

$$\bar{x}_0 = x_k, \quad \text{(C.1}e\text{)}$$

where $\mathbf{u} = [u_0, \ldots, u_{N_c-1}]^\top$ is the control input sequence over the control horizon N_c, which comprises the decision variables of the optimization problem (C.1); N_p is the prediction horizon over which the system behavior is predicted ($N_c \leqslant N_p$); (C.1*a*), (C.1*b*) represent the system model, with $\bar{x}$ and $\bar{z}$ denoting the predicted differential and algebraic state variables, respectively (see (13)); J is the objective function; l denotes (possibly nonlinear) state constraint functions; and $\mathcal{U}$ is a convex, compact set that defines the input constraints. The prediction and control horizons N_p and N_c are commonly treated as the tuning parameters of MPC.

Appendix D. Tuning parameters of PI controllers

Table D1. Tuning parameters of the PI controllers in Case Studies I and II.

Proportional controller (P paired with V_A)	
k_P	-20 V W^{-1}
Proportional integral controller (T_s paired with v_{in})	
k_p	158 m s^{-1} K^{-1}
τ_i	96 s

ORCID

Ali Mesbah https://orcid.org/0000-0002-1700-0600

References

[1] Becker K, Kogelschats U, Schonenbach K and Barker R J 2005 *Non-Equilibrium Air Plasmas at Atmospheric Pressure* (Bristol: Institute of Physics Publishing)

[2] Jeong J Y, Babayan S E, Tu V J, Park J, Henins I, Hicks R F and Selwyn G S 1999 Etching materials with an atmospheric-pressure plasma jet *Plasma Sources Sci. Technol.* **7** 282–5

[3] Chu P, Chen J, Wang L and Huang N 2002 Plasma-surface modification of biomaterials *Mater. Sci. Eng.* R **36** 143–206

[4] Laroussi M, Kong M, Morfill G and Stolz W 2012 *Plasma Medicine* (New York: Cambridge University Press)

[5] Kong M G, Kroesen G, Morfill G, Nosenko T, Shimizu T, van Dijk J and Zimmermann J L 2009 Plasma medicine: an introductory review *New J. Phys.* **11** 115012

[6] Pavlovich M J, Clark D S and Graves D B 2014 Quantification of air plasma chemistry for surface disinfection *Plasma Sources Sci. Technol.* **23** 065036

[7] Metelmann H-R *et al* 2015 Head and neck cancer treatment and physical plasma *Clin. Plasma Med.* **3** 17–23

[8] Isbary G, Zimmermann J L, Shimizu T, Li Y F, Morfill G E, Thomas H M, Steffes B, Heinlin J, Karrer S and Stolz W 2013 Non-thermal plasma-more than five years of clinical experience *Clin. Plasma Med.* **1** 19–23

[9] Kvam E, Davis B, Mondello F and Garner A L 2012 Nonthermal atmospheric plasma rapidly disinfects multidrug-resistant microbes by inducing cell surface damage *Antimicrob. Agents Chemother.* **56** 2028–36

[10] Kalghatgi S, Friedman G, Fridman A and Clyne A M 2010 Endothelial cell proliferation is enhanced by low dose non-thermal plasma through fibroblast growth factor-2 release *Ann. Biomed. Eng.* **38** 748–57

[11] Dobrynin D *et al* 2011 Live pig skin tissue and wound toxicity of cold plasma treatment *Plasma Med.* **1** 93–108

[12] Sapareto S A and Dewey W C 1984 Thermal dose determination in cancer therapy *Int. J. Radiat. Oncol. Biol. Phys.* **10** 787–800

[13] Chen C, Liu D X, Liu Z C, Yang A J, Chen H L, Shama G and Kong M G 2014 A model of plasma-biofilm and plasma-tissue interactions at ambient pressure *Plasma Chem. Plasma Process.* **34** 403–41

[14] Roti Roti J L 2008 Cellular responses to hyperthermia (40–46 degrees C): cell killing and molecular events *Int. J. Hyperth.* **24** 3–15

[15] Wende K *et al* 2015 Identification of the biologically active liquid chemistry induced by a nonthermal atmospheric pressure plasma jet *Biointerphases* **10** 029518

[16] Schutze A, Jeong J Y, Babayan S E, Park J, Selwyn G S and Hicks R F 1998 The atmospheric-pressure plasma jet: a review and comparison to other plasma sources *IEEE Trans. Plasma Sci.* **26** 1685–94

[17] Lu X, Laroussi M and Puech V 2012 On atmospheric-pressure non-equilibrium plasma jets and plasma bullets *Plasma Sources Sci.Technol.* **21** 034005

[18] Jablonowski H, Hänsch M A C, Dünnbier M, Wende M U, Kristian Hammer, Weltmann K-D, Reuter S and Woedtke T V 2015 Plasma jet's shielding gas impact on bacterial inactivation *Biointerphases* **10** 029506

[19] Fridman G, Brooks A D, Balasubramanian M, Fridman A, Gutsol A, Vasilets V N, Ayan H and Friedman G 2007 Comparison of direct and indirect effects of non-thermal atmospheric-pressure plasma on bacteria *Plasma Process. Polym.* **4** 370–5

[20] Hofmann S, van Gils K, van der Linden S, Iseni S and Bruggeman P 2014 Time and spatial resolved optical and electrical characteristics of continuous and time modulated RF plasmas in contact with conductive and dielectric substrates *Eur. Phys. J.* D **68** 56

[21] Sakiyama Y, Graves D B and Stoffels E 2008 Influence of electrical properties of treated surface on RF-excited plasma needle at atmospheric pressure *J. Phys. D: Appl. Phys.* **41** 95204

[22] Dünnbier M, Schmidt-Bleker A, Winter J, Wolfram M, Hippler R, Weltmann K-D and Reuter S 2013 Ambient air particle transport into the effluent of a cold atmospheric-pressure argon plasma jet investigated by molecular beam mass spectrometry *J. Phys. D: Appl. Phys.* **46** 435203

[23] Staack D, Farouk B, Gutsol A and Fridman A 2009 Stabilization of the ionization overheating thermal instability in atmospheric pressure microplasmas *J. Appl. Phys.* **106** 700–11

[24] Morari M and Lee J H 1999 Model predictive control: past, present and future *Comput. Chem. Eng.* **23** 667–82

[25] Rawlings J B and Mayne D Q 2015 *Model Predictive Control: Theory and Design* 5th edn (Madison, WI: Nob Hill)

[26] Garcia C E and Morari M 1982 Internal model control: I. A unifying review and some new results *Ind. Eng. Chem. Process Des. Dev.* **21** 308–23

[27] Edgar T F, Butler S W, Campbell W J, Pfeiffer C, Bode C, Hwang S, Balakrishnan K and Hahn J 2000 Automatic control in microelectronics manufacturing: Practices, challenges, and possibilities *Automatica* **36** 1567–603

[28] Stokes D, Member S, May G S and Member S 2000 Real-time control of reactive ion etching using neural networks *IEEE Trans. Semicond. Manuf.* **13** 469–80

[29] Ringwood J V, Lynn S, Bacelli G, Ma B, Ragnoli E and Mcloone S 2010 Estimation and control in semiconductor etch: practice and possibilities *IEEE Trans. Semicond. Manuf.* **23** 87–98

[30] Albanese R and Ambrosino G 2000 Current, position and shape control of tokamak plasmas: a literature review *IEEE Int. Conf. on Control Applications* pp 385–94

[31] Ambrosino G and Albanese R 2005 Magnetic control of plasma current, position, and shape in tokamaks: a survey of modeling and control approaches *IEEE Control Syst. Mag.* **25** 76–92

[32] Maljaars B, Felici F, de Baar M and Steinbuch M 2015 Model predictive control of the current density distribution and stored energy in tokamak fusion experiments using trajectory linearizations *IFAC-PapersOnLine* **48** 314–21

[33] Haas R A 1973 Plasma stability of electric discharges in molecular gases *Phys. Rev.* A **8** 1017–43

[34] Shi J J, Deng X T, Hall R, Punnett J D and Kong M G 2003 Three modes in a radio frequency atmospheric pressure glow discharge *J. Appl. Phys.* **94** 6303–10

[35] Walsh J L, Iza F, Janson N B, Law V J and Kong M G 2010 Three distinct modes in a cold atmospheric pressure plasma jet *J. Phys. D: Appl. Phys.* **43** 075201

[36] Liu J J and Kong M G 2011 Sub-60C atmospheric heliumwater plasma jets: modes, electron heating and downstream reaction chemistry *J. Phys. D: Appl. Phys.* **44** 345203

[37] Shi J J and Kong M G 2005 Expansion of the plasma stability range in radio-frequency atmospheric-pressure glow discharges *Appl. Phys. Lett.* **87** 1–3

[38] Hsu D D and Graves D B 2003 Microhollow cathode discharge stability with flow and reaction *J. Phys. D: Appl. Phys.* **36** 2898–907

[39] Ang K H, Chong G and Li Y 2005 PID control system analysis, design, and technology *IEEE Trans. Control Syst. Technol.* **13** 559–76

[40] Stoffels E, Kieft I E, Sladek R E J, Bedem L J M V D, Laan E P V D and Steinbuch M 2006 Plasma needle for *in vivo* medical treatment: recent developments and perspectives *Plasma Sources Sci. Technol.* **15** S169–80

[41] Sakiyama Y and Graves D B 2006 Finite element analysis of an atmospheric pressure RF-excited plasma needle *J. Phys. D: Appl. Phys.* **39** 3451–6

[42] Schröder M, Ochoa A and Breitkopf C 2015 Numerical simulation of an atmospheric pressure RF-driven plasma needle and heat transfer to adjacent human skin using COMSOL *Biointerphases* **10** 029508

[43] Balcon N, Hagelaar G J M and Boeuf J P 2008 Numerical model of an argon atmospheric pressure RF discharge *IEEE Trans. Plasma Sci.* **36** 2782–7

[44] Stoffels E, Flikweert A J, Stoffels W W and Kroesen G M W 2002 Plasma needle: a non-destructive atmospheric plasma source for fine surface treatment of (bio)materials *Plasma Sources Sci. Technol.* **11** 383–8

[45] Gidon D, Graves D B and Mesbah A 2016 Model predictive control of thermal effects of an atmospheric pressure plasma jet for biomedical applications *Proc. American Control Conf. (Boston)* pp 4889–94

[46] Pennes H 1948 Analysis of tissue and arterial blood temperatures in the resting human forearm *J. Appl. Physiol.* **85** 5–34

[47] Dewhirst M W, Viglianti B L, Hanson M, Hoopes P J, Viglianti B L, Hanson M and Hoopes P J 2003 Basic principles of thermal dosimetry and thermal thresholds for tissue damage from hyperthermia *Int. J. Hyperth.* **3** 267–94

[48] Heuer K, Hoffmanns M A, Demir E, Baldus S, Volkmar C M, Röhle M, Fuchs P C, Awakowicz P, Suschek C V and Opländer C 2015 The topical use of non-thermal dielectric barrier discharge DBD: nitric oxide related effects on human skin *Nitric Oxide* **44** 52–60

[49] Gaur N, Szili E J, Oh J-S, Hong S-H, Michelmore A, Graves D B, Hatta A and Short R D 2015 Combined effect of protein and oxygen on reactive oxygen and nitrogen species in the plasma treatment of tissue *Appl. Phys. Lett.* **107** 103703

[50] Vandamme M *et al* 2012 ROS implication in a new antitumor strategy based on non-thermal plasma *Int. J. Cancer* **130** 2185–94

[51] Cheng X, Sherman J, Murphy W, Ratovitski E, Canady J and Keidar M 2014 The effect of tuning cold plasma composition on glioblastoma cell viability *PLoS One* **9** 1–9

[52] Kim H J, Shim D H and Sastry S 2002 Nonlinear model predictive tracking control for rotorcraft-based unmanned aerial vehicles *Proc. American Control Conf. (Anchorage, AK)* pp 3576–81

[53] Qin S and Badgwell T A 2003 A survey of industrial model predictive control technology *Control Eng. Pract.* **11** 733–64

[54] Klancar G and Skrjanc I 2007 Tracking-error model-based predictive control for mobile robots in real time *Robot. Auton. Syst.* **55** 460–9

[55] Ma Y, Borrelli F, Hencey B, Coffey B, Bengea S and Haves P 2012 Model predictive control for the operation of building cooling systems *IEEE Trans. Control Syst. Technol.* **20** 796–803

[56] Wächter A and Biegler L T 2006 On the implementation of an interior-point filter line-search algorithm for large-scale nonlinear programming *Math. Program.* **106** 25–57

[57] Åström K J and Hägglund T 1995 *PID Controllers: Theory, Design, and Tuning* (Research Triangle Park, NC: Instrument Society of America)

[58] Pannocchia G and Rawlings J B 2003 Disturbance models for offset-free model predictive control *AIChE J.* **49** 426–37

[59] Lieberman M and Lichtenberg A J 2005 *Principles of Plasma Discharges and Materials Processing* (Hoboken, NJ: Wiley)

[60] Lieberman M 2015 Analytical model of atmospheric pressure, helium/trace gas radio-frequency capacitive Penning discharges *Plasma Sources Sci.Technol.* **24** 025009

[61] Shi J J and Kong M G 2005 Mechanisms of the α and γ modes in radio-frequency atmospheric glow discharges *J. Appl. Phys.* **97** 023306